ACS APPLIED MATERIALS & INTERFACES

www.acsami.org

Research Article

Tuning Rate-Limiting Factors to Achieve Ultrahigh-Rate Solid-State Sodium-Ion Batteries

Zijian Wang,[†] Luyi Yang,[†] Jiajie Liu,[†] Yongli Song, Qinghe Zhao, Kai Yang, and Feng Pan*

Cite This: *ACS Appl. Mater. Interfaces* 2020, 12, 48677−48683

Read Online

ACCESS | Metrics & More | Article Recommendations | Supporting Information

ABSTRACT: Exhibiting superior safety features and low costs, solid-state sodium (Na)-ion batteries have been proposed as an attractive candidate for energy storage. However, the poor rate capability of solid-state batteries has limited their applications. In this work, an all-solid-state Na-ion battery is fabricated, delivering an unprecedented rate capability (60% capacity retention at a C-rate of 100 C with an areal loading of 1.5 mg cm^{-2}), which far exceeds other reports so far. More importantly, it is further demonstrated that instead of the Na-ion conductivity of the solid electrolyte, the rate-limiting factors are determined to be charge-transfer resistance at electrode/solid electrolyte interfaces and lack of percolation pathways in the electrode, which can be optimized by tuning the electrode design and testing protocols.

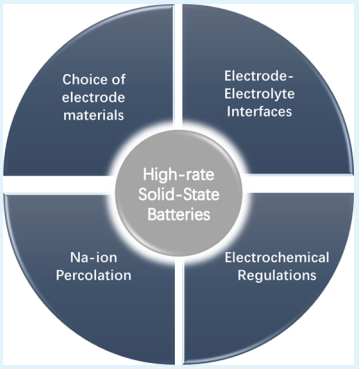

KEYWORDS: *solid-state batteries, sodium-ion batteries, high-rate performance, PEO, interfaces*

1. INTRODUCTION

Among all energy storage devices, rechargeable lithium-ion batteries (LIBs) are the dominant commercialized products because of their excellent cycling stability and energy density.[1−3] Owing to the limited resource and high cost of lithium, sodium-ion batteries (SIBs) have become a promising alternative to LIBs because of their natural abundance and suitable redox potential.[4−6] Exhibiting superior safety features and low costs, solid-state SIBs have been proposed as an attractive candidate for energy storage with lower cost and better safety compared to traditional lithium-ion batteries. In order to meet the demands of high-performance electronic devices, one of the major challenges faced with solid-state batteries (SSBs) is to improve their rate capability.[7]

The first key factor toward better rate capability is choosing appropriate host materials for Na^+ with superior electrochemical kinetics. Adopted from the Li analogue, Na-based layered oxides[8] and phosphates[9] have been widely studied as the cathode materials for SIBs. Because the radius of Na^+ (1.02 Å) is much larger than that of Li^+ (0.76 Å), its sluggish reaction kinetics in traditional insertion-based cathode materials have severely hindered the rate performances for solid-state SIBs. Prussian blue analogues (PBAs) are considered as suitable hosts for Na^+ storage because of the large interstitial "A" sites (4.6 Å) and ionic channels (3.2 Å in the ⟨100⟩ direction) in their lattices,[10] resulting in high sodium-ion diffusion coefficients.[11,12] As for anode materials, although nongraphite carbons[13−15] and alloys[16] generally show high specific capacities and low working potential, their intrinsically poor rate capability have made them unsuitable for solid-state SIBs. Although the Na metal anode has been considered as a competitive candidate for SSBs because of its high specific capacity of 1166 mA h g^{-1}, issues such as unstable Na/electrolyte interfaces[17−20] and relatively low melting point of sodium metal (97.8 °C) could raise practical difficulties during application. Alternatively, $KTi_2(PO_4)_3$ (KTP) has shown superior rate performances for Na^+ storage, also owing to its larger channels for Na^+ diffusion.[21]

Intuitively, another approach is to design and prepare solid electrolytes with higher ionic conductivity. However, SSBs with excellent rate capability have yet to be reported, even though the conductivity has been improved to as high as 12 mS cm^{-1} at room temperature.[22] This may be attributed to the contact condition between active materials and solid electrolytes, especially for inorganic solid electrolytes, which are normally rigid and create large charge transfer resistance, leading to poor rate performance.[23] In addition, some SSEs suffer from chemically unstable interfaces[24−26] and low critical current densities.[27,28] Alternatively, solid polymer electrolytes exhibit good permeability at elevated temperatures, hence the better interfacial contacting properties with electrodes.[29]

Received: August 20, 2020
Accepted: October 6, 2020
Published: October 16, 2020

https://dx.doi.org/10.1021/acsami.0c15015
ACS Appl. Mater. Interfaces 2020, 12, 48677−48683

Therefore, they are considered a more practical choice for high-rate-performance SSBs.

In this work, by coupling a Na-ion-based polyethylene oxide (PEO) solid-state electrolyte (PEONa) with the nanosized potassium-based PBA (KPBA) cathode and KTP anode, an all-solid-state SIB system is proposed and tested. Interestingly, an unprecedented rate capability is achieved despite the relatively low Na-ion conductivity in PEONa, suggesting that an ultrahigh ionic conductivity is not a must. As a result, as presented in Scheme 1, the choices of electrode materials, the electrode/electrolyte interface, and Na-ion diffusion within electrodes and electrochemical testing conditions are proposed as rate-determining aspects for high-rate solid-state batteries.

Scheme 1. Rate-determining Aspects for High-Rate Solid-State Batteries

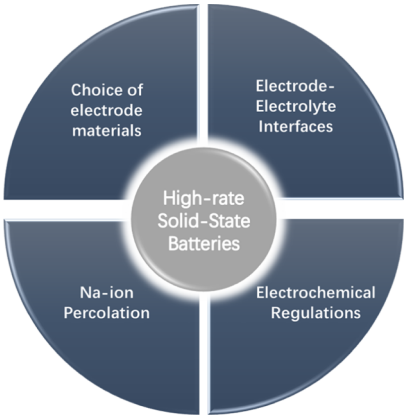

2. EXPERIMENTAL SECTION

2.1. Synthesis of KTP@C. Phosphoric acid (3 mmol) and 1 mmol of potassium acetate were dissolved in 30 mL of ethanol and 30 mL of ethylene glycol by stirring. Then, 2 mmol of tetrabutyl titanate was added into the solution followed by 2 h of stirring. The precipitated precursor was obtained by centrifugation and washed with ethanol and then dried at 80 °C overnight. The black KTP@C powder was obtained by sintering the precursor at 750 °C in an Ar atmosphere for 2 h.

2.2. Synthesis of KPBA. KPBA is prepared by first dissolving 15.4 mmol of potassium citrate monohydrate and 6 mmol of $FeSO_4 \cdot 7H_2O$ in 100 mL of deionized water, followed by vigorous stirring under a N_2 atmosphere. Then, 100 mL of aqueous solution containing 4 mmol of $K_4Fe(CN)_6 \cdot 3H_2O$ was slowly added into the previous solution with vigorous stirring under a N_2 atmosphere overnight. The white precipitate was obtained by centrifugation followed by freeze-drying.

2.3. Synthesis of PEONa. PEO (Dow Chemical Company, M_w = 4 M, 0.3 g), 0.042 g of $NaClO_4$ (99.99%, Aladdin), and 0.015 g of nano-Al_2O_3 (Aladdin) were mixed and stirred in anhydrous acetonitrile for 6 h. The resultant slurry was cast on a Teflon mold and dried into a membrane in an Ar-filled glovebox. The membrane was then dried at 65 °C before use. The thickness of the as-prepared PEONa membranes is approximately 50 μm.

2.4. Material Characterization. Crystallographic information was obtained using a Bruker D8 ADVANCE powder X-ray diffractometer with a Cu Kα X-ray source. Field-emission scanning electron microscopy (SEM) was performed on a Zeiss SUPRA-55 microscope. Transmission electron microscopy (TEM) images were collected using a JEM-3200FS (JEOL) microscope. The inductively coupled plasma (ICP) analysis was carried out using an ICP-AES (JY2000-2).

2.5. Electrochemical Test. A total of 2032 coin cells were used in all electrochemical tests, and all cells were fabricated in a glovebox in an Ar atmosphere. The electrodes were prepared by slurry casting, where the weight ratio of the active material (i.e., KTP and KPBA), conductive material (acetylene black), and binder [polyvinylidene difluoride (PVDF)] was 5:3:2. For solid-state cells, the cathode, PEONa membrane, and anode were sandwiched in the coin cell. For cells using the liquid electrolyte, 1 M solution of $NaClO_4$ in ethylene carbonate (EC)/diethylene carbonate (DEC) (1:1 w/w) with 5 wt % of fluoroethylene carbonate (FEC) was used as the liquid electrolyte and Whatman glass fiber (GF/C) was used as the separator. Galvanostatic cycling was performed on an automatic charge–discharge unit (Land Electronic). Other electrochemical tests were performed on a Solartron 1400 CellTest system. The diffusion coefficient of Na^+ in PEO was measured by applying a constant current of 0.2 mA on a Na symmetric cell and measuring the voltage change.

3. RESULTS AND DISCUSSION

3.1. Material Characterizations. The X-ray diffraction (XRD) patterns of the prepared electrode materials are shown in Figure 1a,b, both of which can be well indexed to the standard patterns of KTP and monoclinic KPBA. It is noteworthy that in Figure 1b, the peak widths are broad, inferring small particle sizes for KPBA. From the SEM images of KTP (Figure 1c) and KPBA (Figure 1d), it can be observed that KTP displays spherical morphology and an interconnecting structure with an average particle size of approximately 175 nm. In comparison, PBA shows a much smaller average size of approximately 10–20 nm, which explains its poor crystallinity from the XRD result. The TEM image of KTP (Figure S1a) exhibits a homogeneous thin carbon coating of 2 nm on the particle surface, which is beneficial to its electronic conductivity.[21] From the TEM image of KPBA (Figure S1b), it can be observed that the synthesized KPBA consists of nanosized (approximately 10 nm) crystalline domains, which is consistent with its broad XRD peaks. Using ICP spectroscopy, the chemical composition of the prepared KPBA is determined to be $K_{2.01}Fe_2(CN)_6$, which is ideal for Na-deficient anodes such as KTP. In addition, from the results of thermogravimetric analysis at 120 and 180 °C (shown in Figure S2), the total weight percentage of water in KPBA is estimated to be 13.9%. The Arrhenius plot (Figure 1e) shows that when [EO]/[Na^+] = 20, PEONa exhibits the highest ionic conductivity (4.79×10^{-4} S cm^{-1}) at 80 °C. Therefore, this ratio is adopted throughout this work. All tests of solid-state cells were carried out at 80 °C unless specified otherwise. Cyclic voltammogram (CV) of KPBA/Na and KTP/Na cells (Figure S3a) in solid-state half-cells shows redox peaks at 2.08 and 2.17 V, respectively, corresponding to a reversible Na-ion insertion/extraction reaction. The CV curves of KBPA (Figure S3b) exhibit two oxidation peaks (3.10 and 3.76 V) and two reduction peaks (2.84 and 3.47 V), which can be ascribed to a $2e^-$ electrochemical reaction.

Because the K ion will deintercalate from KPBA during the first charge, it is important to investigate the intercalation behaviors of K and Na ions in KPBA and KTP. Therefore, ICP measurements are carried out for both materials after different cycle numbers with the liquid electrolyte (1 M $NaClO_4$ in EC/DEC = 1:1 with 5% FEC). It can be seen from Figure S4, for KPBA, that the molar ratio of Na and K increases with the cycle number, indicating that Na-ion insertion behavior is dominant in KPBA. In addition, it is shown that by replacing $NaClO_4$ with $KClO_4$ in the liquid electrolyte, the KTP/K half-

https://dx.doi.org/10.1021/acsami.0c15015
ACS Appl. Mater. Interfaces 2020, 12, 48677–48683

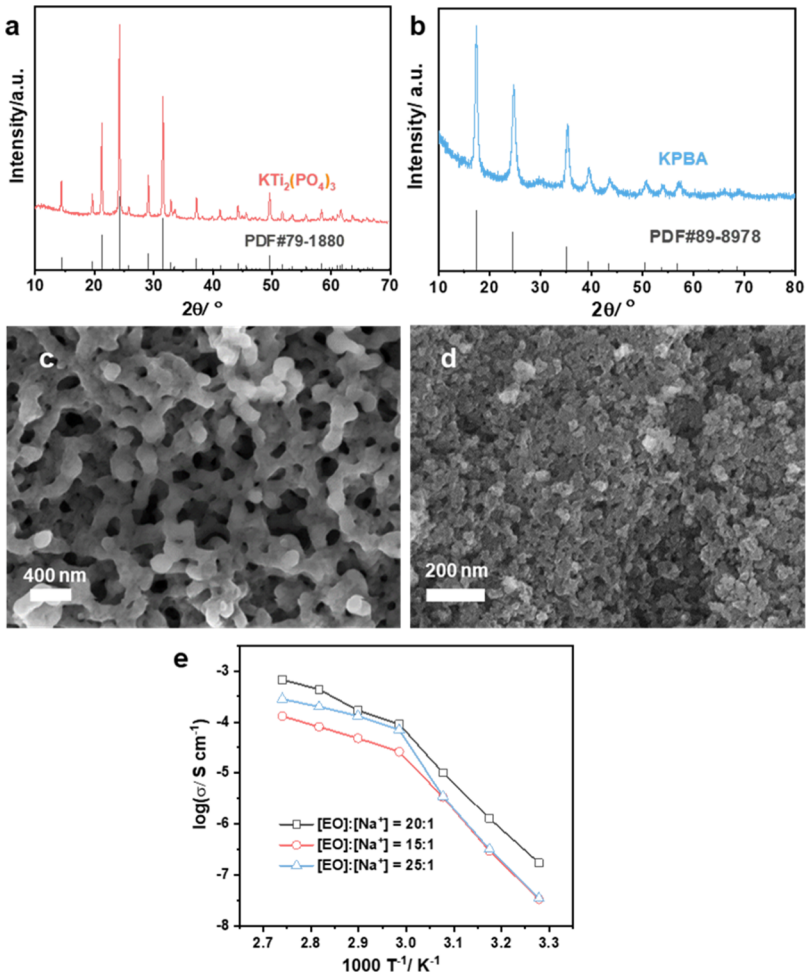

Figure 1. XRD patterns of KTP (a) and PBA (b); SEM images of KTP (c) and KPBA (d). The Arrhenius plot of PEONa with different [EO]/[Na^+] ratios (e).

cell exhibits very poor electrochemical performance (as shown in Figure S5a), suggesting poor insertion capability of the K ion in the anode. This conclusion is also well supported by the poor electrochemical performance of the solid battery using a K-ion-based solid electrolyte (PEOK) (shown in Figure S5b).

3.2. Galvanostatic Cycling Tests. Next, the rate performance of the KPBA-PEONa-KTP cell is evaluated. The potential profiles of the cell at different C-rates are presented in Figure 2a. It can be seen that at 1 C (100 mA g^{-1}), two distinctive plateaus can be observed around 0.9 and 1.5 V, suggesting the redox reactions for two different Fe ions. However, as the current density gradually increases, the plateau at 1.5 V is shortened from 40 mA h g^{-1} at 1 C to virtually zero at 100 C, whereas the plateau at 0.9 V is retained to be approximately 60 mA h g^{-1} at 100 C. Figure 2b shows that an unprecedented rate performance for the solid-state battery is obtained: average capacities of 121, 115,102, 92, 84, 78, and 73 mA h g^{-1} can be obtained at 1, 2, 5, 10, 20, 50, and 100 C, respectively. In comparison, the KPBA-PEONa-Na cell delivers much lower capacities. The superior rate capability of the KTP anode compared to Na metal can be attributed to the lower charge transfer resistance (R_{CT}, represented by the semicircles in the Nyquist plot) in Figure 2c. From this result, it can be inferred that even for PEO, which is considered to exhibit good wetting ability at electrolyte/electrode interfaces, the charge transfer between Na and SSE can also be the rate-determining step for high-rate cycling. Interestingly, it is also found that the KPBA-KTP cell using the liquid electrolyte (1 M $NaClO_4$ in EC/DEC = 1:1 with 5 wt % FEC) exhibits a very low first-cycle capacity of 25 mA h g^{-1} compared to the solid-state cell (see Figure 2d). ICP results further show that after immersing KPBA in the traditional liquid electrolyte overnight, the molar ratio of K/Fe decreases dramatically from almost unity to 0.41 (Figure 2d), suggesting severe K-ion dissolution in the liquid electrolyte, hence the low capacity. Such a dissolution effect might be more severe for nanosized active materials compared with larger particles. Therefore, it can be inferred that the solid electrolyte such as PEO is ideal for full-cell systems using the Na (Li)-deficient anode. Moreover, the cycling performance of the KPBA-PEONa-KTP cell was also examined. As exhibited in Figure 2e, at a rate of 20 C, the Coulombic efficiencies are retained over 97% for over 6000 cycles and 62.7% of reversible capacity can be obtained, indicating excellent cycling stability.

3.3. Promoting Ion Transfer in the Electrode. As stated above, solid electrolytes tend to wet the active material less well than liquid electrolytes because of the lack of flow. Therefore, how to construct fast ion-transfer pathways within the electrode will be a critical challenge, especially when a thick electrode is employed to pursue higher energy densities. Therefore, compared with pursuing high ionic conductivities, boosting ion transfer within the electrode should be equally important, if not more so.

https://dx.doi.org/10.1021/acsami.0c15015
ACS Appl. Mater. Interfaces 2020, 12, 48677−48683

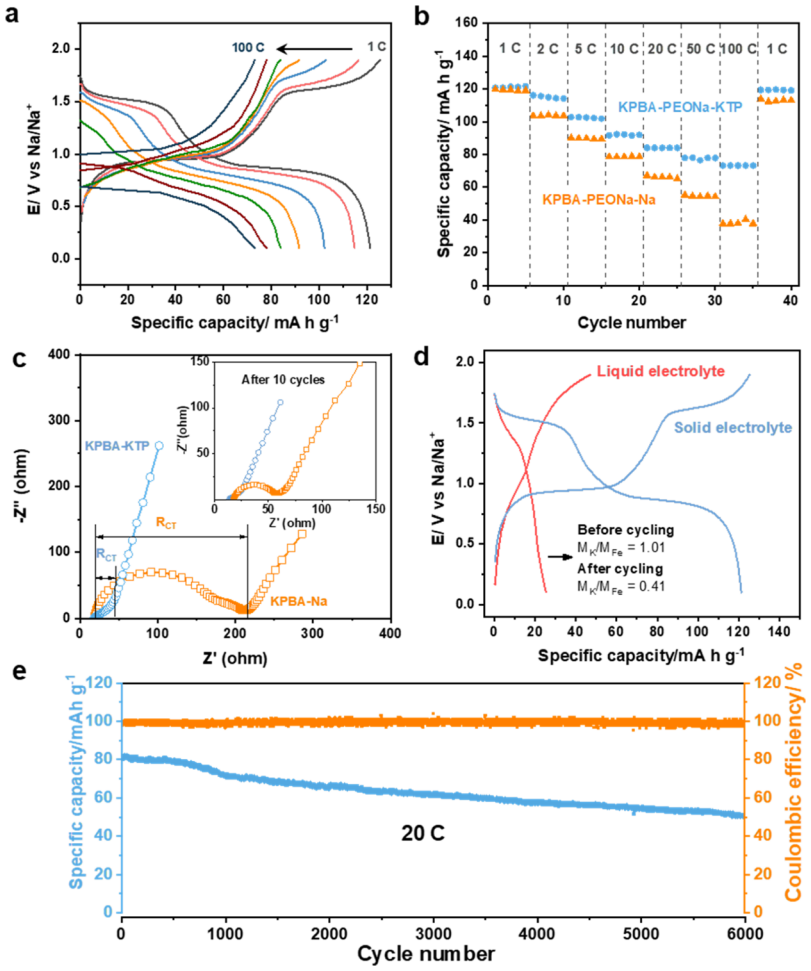

Figure 2. (a) Voltage profiles of the KPBA-PEONa-KTP cell under various C-rates; (b) rate performance of KPBA-PEONa-KTP and KPBA-PEONa-Na cells; (c) electrochemical impedance spectra of KPBA-PEONa-KTP and KPBA-PEONa-Na cells before cycling and after 10 cycles (inset); (d) first-cycle voltage profiles of KPBA-KTP cells using the solid-state electrolyte and liquid electrolyte at a rate of 1 C; (e) cycling performance at 20 C. The areal loading of the KPBA positive electrode is 0.3 mg cm^{-2}, coupled with approximately 10% excess of KTP in the negative electrode. All tests are carried out at 80 °C.

First, the impact of ionic conductivity on the solid electrolyte is evaluated. Because PEO-based SSEs exhibit tunable ionic conductivity at different temperatures, they are perfectly suitable for such experiments. By decreasing the temperature from 80 to 65 °C (which is approximately the melting point of PEO), the ionic conductivity decreases by four times from 4.79×10^{-4} to 1.22×10^{-4} S cm^{-1} (as estimated from Figure 1e). In addition, a lower testing temperature generally leads to slower reaction kinetics of the electrode material. Therefore, the rate performance of the solid-state cell at 65 °C is expected to significantly underperform compared with that at 80 °C. However, Figure 3a shows that at 65 °C, the rate performance is not much affected compared to that at 80 °C. This might be due to the fact that even at 65 °C, the diffusion coefficient of Na^+ in PEONa is estimated as high as 2.4×10^{-8} cm^2 s^{-1}, according to the method proposed by Ma et al. (see Figure S6 for details).[30] Therefore, the ion transfer rate in the SSE is not the rate-determining step if it matches with both the cathode (10^{-9} to 10^{-8} cm^2 s^{-1})[11,12] and anode materials (10^{-11} to 10^{-9} cm^2 s^{-1}).[21] Next, the impact of ion transfer within the electrode is evaluated by increasing the areal loading of active materials from 0.3 to 1.5 mg cm^{-2} for both positive and negative electrodes. From Figure 3b, it can be seen that if PVDF is solely used as the binder, rate performance of the thick electrode (101 mA h g^{-1} at 1 C and 47 mA h g^{-1} at 10 C) is far worse compared to the thin one. This can be attributed to the lack of percolation network for the electrolyte. Consequently, the lack of Na-ion pathways within the electrode causes large concentration polarization and further impedes ion transfer during fast charge−discharge processes. In comparison, after adding PEONa to the electrode as a cobinder, the rate performance is greatly promoted (118 mA h g^{-1} at 1 C and 86 mA h g^{-1} at 10 C). Based on a semi-infinite diffusion model, the overall Na-ion diffusion coefficient can be roughly estimated based on the Nyquist plot (Figure S7, detailed steps are described in the Supporting Information). As a result, D_{Na} in the cell using PEONa-PVDF as a binder is calculated to be approximately five times that in the cell using PVDF as the binder. Therefore, as demonstrated in Figure 3c, it can be concluded that Na-ion diffusion is relatively fast in the PEO; however, it becomes sluggish because of the lack of the ion-conducting network in the thick electrode. Hence, the effective capacity is compromised especially at large current densities. In contrast, the presence of PEONa provides additional Na-ion pathways within the electrode, which effectively enable the fast charge transfer process in the thick electrode.

https://dx.doi.org/10.1021/acsami.0c15015
ACS Appl. Mater. Interfaces 2020, 12, 48677−48683

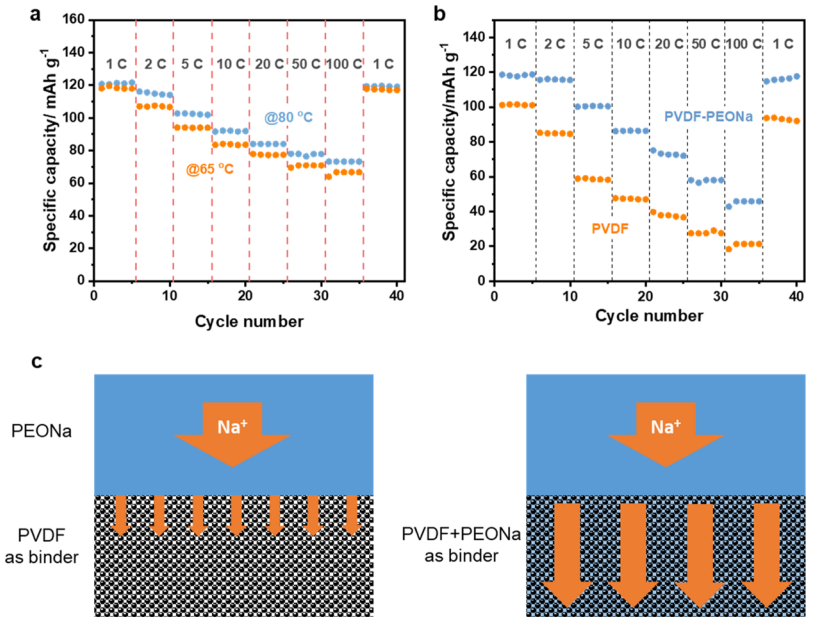

Figure 3. (a) Rate performances of KPBA-PEONa-KTP cells at different temperatures; (b) rate performance of KPBA-PEONa-KTP cells using different binders for thicker electrodes (1.5 mg cm^{-2}); (c) proposed Na-ion transport mechanisms in the electrolyte and the electrode using PVDF (left) and PVDF + PEONa as the binder (right).

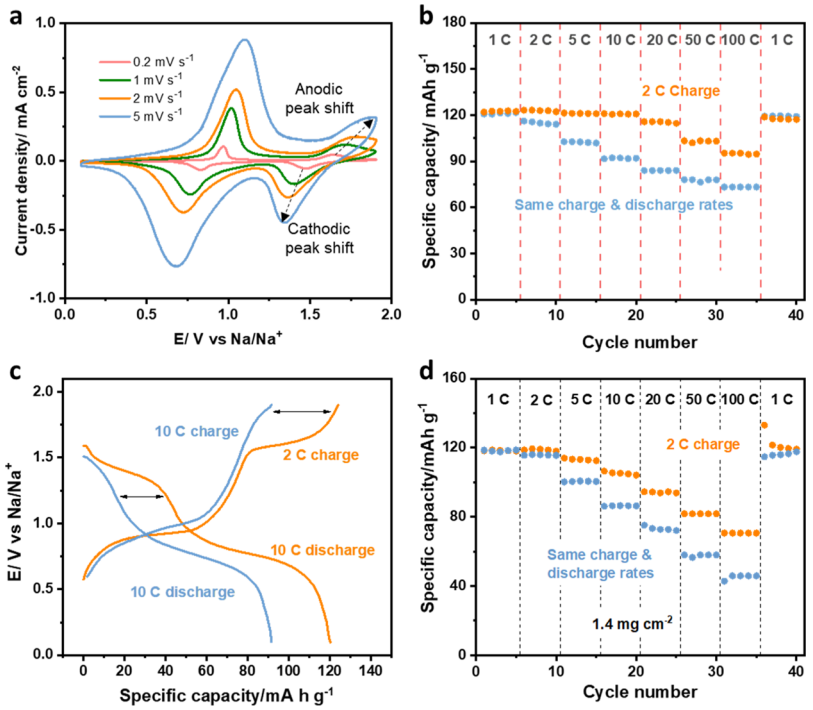

Figure 4. (a) CV curves of the KPBA-PEONa-KTP cell at different scan rates; (b) rate performance and (c) voltage profiles of the KPBA-PEONa-KTP cell with lower areal loading (0.3 mg cm^{-2}) under the same charge−discharge rates and a constant charge rate of 2 C; (d) rate performance of the KPBA-PEONa-KTP cell with higher areal loading (1.5 mg cm^{-2}) under same charge−discharge rates and a constant charge rate of 2 C.

3.4. Electrochemical Regulation. Because most intercalation reaction-based electrode materials have asymmetric ion intercalation and deintercalation kinetics, electrochemical regulation of their charging−discharging conditions can be a promising approach to further optimize their rate performance. From Figure 3a, it can be clearly observed that as the C-rate increases, the capacity loss is mainly contributed by the higher voltage plateau around 1.6 V. Therefore, in order to obtain higher capacity at high rates, it is necessary to identify the origin of such capacity loss at higher rates. From the CV curve of the KPBA-PEONa-KTP cell in Figure 4a, it can be clearly observed that all current peak positions shift with a higher scan rate, suggesting that these electrochemical processes are not completely reversible. By comparing the degrees of peak shift, which reflect the reversibility of an electrochemical process,[31] at 1.6 V for both anodic and cathodic scan, the anodic scanning process exhibits larger peak shift compared to the cathodic one. This result suggests that the charging process for

https://dx.doi.org/10.1021/acsami.0c15015
ACS Appl. Mater. Interfaces 2020, 12, 48677−48683

the plateau at 1.6 V might be the rate-limiting step. In order to verify this assumption, the rate performance is examined under a special testing condition where the charging rate is fixed at 2 C, which is able to meet the fast-charging demand for electric vehicles and electronic devices.[6] It can be seen from Figure 4b that using this cycling protocol, much higher discharge capacities can be obtained at the same rate. The capacity remains almost unchanged at a discharge rate of 10 C (120 mA h g^{-1}), which is much higher than that of the cell using the normal testing method (92 mA h g^{-1}). Even at 100 C, a capacity as high as 94.5 mA h g^{-1} can be achieved. From the voltage profiles exhibited in Figure 4c, it can be seen that at 10 C, the improvement in capacity is mainly contributed by the higher voltage plateau, which supports the previous assumption that the lost capacity around 1.6 V can be recovered by applying a relatively slow charge current density. This cycling protocol was then applied to thick electrodes in order to further optimize the cell performance. From Figure 4d, the rate performance of the cell using the thick electrode is greatly boosted through adopting this charging−discharging protocol: at a rate of 100 C, the capacity is improved from 46 to 71 mA h g^{-1}.

4. CONCLUSIONS

In this study, an all-solid-state SIB system is proposed using nano-sized KPBA as the cathode material, KTP as the anode, and PEONa as the solid-state electrolyte, which exhibits state-of-the-art rate capability (see the comparisons with other research articles listed in Figure 5 and Table S1) and good

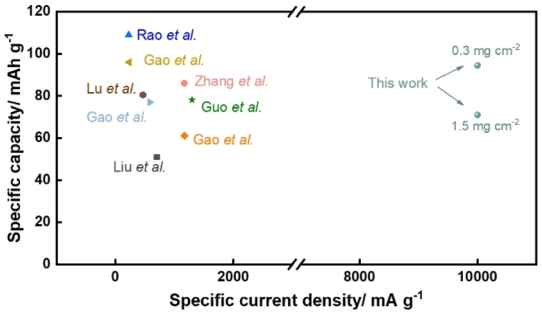

Figure 5. Rate performances of solid-state SIBs reported in recent years. Detailed comparisons are listed in Table S1.

cycling stability (62.7% capacity retention after 6000 cycles at 20 C). It should be noted that PEO can only work at elevated temperatures; future work should focus on developing room-temperature SSBs. Furthermore, by exploring the limiting factors such as the electrode/electrolyte interface, Na-ion diffusion within electrodes, and electrochemical testing conditions, the rate performance of the solid-state battery can be further optimized. As a result, the cell delivers a capacity of 71 mA h g^{-1} at 100 C (60% capacity retention compared to 1 C) at an areal loading of 1.5 mg cm^{-2}. This work provides inspiration for the design and optimization of all-solid-state batteries with extraordinary rate performances.

ASSOCIATED CONTENT

Supporting Information

The Supporting Information is available free of charge at https://pubs.acs.org/doi/10.1021/acsami.0c15015.

Characterizations, electrochemical measurements, and battery performance (PDF)

AUTHOR INFORMATION

Corresponding Author

Feng Pan − *School of Advanced Materials, Peking University, Shenzhen Graduate School, Shenzhen 518055, People's Republic of China;* orcid.org/0000-0002-8216-1339; Email: panfeng@pkusz.edu.cn

Authors

Zijian Wang − *School of Advanced Materials, Peking University, Shenzhen Graduate School, Shenzhen 518055, People's Republic of China*

Luyi Yang − *School of Advanced Materials, Peking University, Shenzhen Graduate School, Shenzhen 518055, People's Republic of China;* orcid.org/0000-0002-5516-9829

Jiajie Liu − *School of Advanced Materials, Peking University, Shenzhen Graduate School, Shenzhen 518055, People's Republic of China*

Yongli Song − *School of Advanced Materials, Peking University, Shenzhen Graduate School, Shenzhen 518055, People's Republic of China*

Qinghe Zhao − *School of Advanced Materials, Peking University, Shenzhen Graduate School, Shenzhen 518055, People's Republic of China*

Kai Yang − *School of Advanced Materials, Peking University, Shenzhen Graduate School, Shenzhen 518055, People's Republic of China*

Complete contact information is available at: https://pubs.acs.org/10.1021/acsami.0c15015

Author Contributions

†ZW, L.Y., and J.L. contributed equally to this work.

Notes

The authors declare no competing financial interest.

ACKNOWLEDGMENTS

This work was financially supported by grants from the National Key R&D Program of China (2016YFB0700600), the National Natural Science Foundation of China (no. 51672012), the China Postdoctoral Science Foundation (2019M660317), and the Shenzhen Science and Technology Research Grant (JCYJ20170818085823773 and ZDSYS201707281026184).

REFERENCES

(1) Owen, J. R. Rechargeable Lithium Batteries. *Chem. Soc. Rev.* **1997**, *26*, 259−267.

(2) Armand, M.; Tarascon, J.-M. Building Better Batteries. *Nature* **2008**, *451*, 652−657.

(3) Yang, L.; Yang, K.; Zheng, J.; Xu, K.; Amine, K.; Pan, F. Harnessing the Surface Structure to Enable High-Performance Cathode Materials for Lithium-Ion Batteries. *Chem. Soc. Rev.* **2020**, *49*, 4667−4680.

(4) Kim, S.-W.; Seo, D.-H.; Ma, X.; Ceder, G.; Kang, K. Electrode Materials for Rechargeable Sodium-Ion Batteries: Potential Alternatives to Current Lithium-Ion Batteries. *Adv. Energy Mater.* **2012**, *2*, 710−721.

(5) Palomares, V.; Casas-Cabanas, M.; Castillo-Martínez, E.; Han, M. H.; Rojo, T. Update on Na-Based Battery Materials. A Growing Research Path. *Energy Environ. Sci.* **2013**, *6*, 2312.

(6) Xiang, J.; Yang, L.; Yuan, L.; Yuan, K.; Zhang, Y.; Huang, Y.; Lin, J.; Pan, F.; Huang, Y. Alkali-Metal Anodes: From Lab to Market. *Joule* **2019**, *3*, 2334−2363.
(7) Manthiram, A.; Yu, X.; Wang, S. Lithium Battery Chemistries Enabled by Solid-State Electrolytes. *Nat. Rev. Mater.* **2017**, *2*, 16103.
(8) Han, M. H.; Gonzalo, E.; Singh, G.; Rojo, T. A Comprehensive Review of Sodium Layered Oxides: Powerful Cathodes for Na-Ion Batteries. *Energy Environ. Sci.* **2015**, *8*, 81−102.
(9) Fang, Y.; Zhang, J.; Xiao, L.; Ai, X.; Cao, Y.; Yang, H. Phosphate Framework Electrode Materials for Sodium Ion Batteries. *Adv. Sci.* **2017**, *4*, 1600392.
(10) Qian, J.; Wu, C.; Cao, Y.; Ma, Z.; Huang, Y.; Ai, X.; Yang, H. Prussian Blue Cathode Materials for Sodium-Ion Batteries and Other Ion Batteries. *Adv. Energy Mater.* **2018**, *8*, 1702619.
(11) Takachi, M.; Fukuzumi, Y.; Moritomo, Y. Na^+ Diffusion Kinetics in Nanoporous Metal-Hexacyanoferrates. *Dalton Trans.* **2016**, *45*, 458−461.
(12) Shibata, T.; Moritomo, Y. Ultrafast Cation Intercalation in Nanoporous Nickel Hexacyanoferrate. *Chem. Commun.* **2014**, *50*, 12941−12943.
(13) Hou, H.; Qiu, X.; Wei, W.; Zhang, Y.; Ji, X. Carbon Anode Materials for Advanced Sodium-Ion Batteries. *Adv. Energy Mater.* **2017**, *7*, 1602898.
(14) Li, Y.; Hu, Y.-S.; Titirici, M.-M.; Chen, L.; Huang, X. Hard Carbon Microtubes Made from Renewable Cotton as High-Performance Anode Material for Sodium-Ion Batteries. *Adv. Energy Mater.* **2016**, *6*, 1600659.
(15) Bai, P.; He, Y.; Zou, X.; Zhao, X.; Xiong, P.; Xu, Y. Elucidation of the Sodium-Storage Mechanism in Hard Carbons. *Adv. Energy Mater.* **2018**, *8*, 1703217.
(16) Lao, M.; Zhang, Y.; Luo, W.; Yan, Q.; Sun, W.; Dou, S. X. Alloy-Based Anode Materials toward Advanced Sodium-Ion Batteries. *Adv. Mater.* **2017**, *29*, 1700622.
(17) Wenzel, S.; Leichtweiss, T.; Weber, D. A.; Sann, J.; Zeier, W. G.; Janek, J. Interfacial Reactivity Benchmarking of the Sodium Ion Conductors $Na_3PS_4$and Sodium β-Alumina for Protected Sodium Metal Anodes and Sodium All-Solid-State Batteries. *ACS Appl. Mater. Interfaces* **2016**, *8*, 28216−28224.
(18) Chen, X.; Shen, X.; Li, B.; Peng, H. J.; Cheng, X. B.; Li, B. Q.; Zhang, X. Q.; Huang, J. Q.; Zhang, Q. Ion−Solvent Complexes Promote Gas Evolution from Electrolytes on a Sodium Metal Anode. *Angew. Chem., Int. Ed.* **2018**, *57*, 734−737.
(19) Tang, H.; Deng, Z.; Lin, Z.; Wang, Z.; Chu, I.-H.; Chen, C.; Zhu, Z.; Zheng, C.; Ong, S. P. Probing Solid-Solid Interfacial Reactions in All-Solid-State Sodium-Ion Batteries with First-Principles Calculations. *Chem. Mater.* **2018**, *30*, 163−173.
(20) Mogensen, R.; Brandell, D.; Younesi, R. Solubility of the Solid Electrolyte Interphase (SEI) in Sodium Ion Batteries. *ACS Energy Lett.* **2016**, *1*, 1173−1178.
(21) Sheng, J.; Peng, C.; Xu, Y.; Lyu, H.; Xu, X.; An, Q.; Mai, L. $KTi_2(PO_4)_3$ with Large Ion Diffusion Channel for High-Efficiency Sodium Storage. *Adv. Energy Mater.* **2017**, *7*, 1700247.
(22) Kamaya, N.; Homma, K.; Yamakawa, Y.; Hirayama, M.; Kanno, R.; Yonemura, M.; Kamiyama, T.; Kato, Y.; Hama, S.; Kawamoto, K.; Mitsui, A. A Lithium Superionic Conductor. *Nat. Mater.* **2011**, *10*, 682−686.
(23) Kerman, K.; Luntz, A.; Viswanathan, V.; Chiang, Y.-M.; Chen, Z. Review—Practical Challenges Hindering the Development of Solid State Li Ion Batteries. *J. Electrochem. Soc.* **2017**, *164*, A1731−A1744.
(24) Yang, L.; Song, Y.; Liu, H.; Wang, Z.; Yang, K.; Zhao, Q.; Cui, Y.; Wen, J.; Luo, W.; Pan, F. Stable Interface between Lithium and Electrolyte Facilitated by a Nanocomposite Protective Layer. *Small Methods* **2020**, *4*, 1900751.
(25) Tian, Y.; Shi, T.; Richards, W. D.; Li, J.; Kim, J. C.; Bo, S.-H.; Ceder, G. Compatibility Issues between Electrodes and Electrolytes in Solid-State Batteries. *Energy Environ. Sci.* **2017**, *10*, 1150−1166.
(26) Tian, Y.; Sun, Y.; Hannah, D. C.; Xiao, Y.; Liu, H.; Chapman, K. W.; Bo, S.-H.; Ceder, G. Reactivity-Guided Interface Design in Na Metal Solid-State Batteries. *Joule* **2019**, *3*, 1037−1050.
(27) Song, Y.; Yang, L.; Tao, L.; Zhao, Q.; Wang, Z.; Cui, Y.; Liu, H.; Lin, Y.; Pan, F. Probing into the Origin of an Electronic Conductivity Surge in a Garnet Solid-State Electrolyte. *J. Mater. Chem. A* **2019**, *7*, 22898−22902.
(28) Song, Y.; Yang, L.; Zhao, W.; Wang, Z.; Zhao, Y.; Wang, Z.; Zhao, Q.; Liu, H.; Pan, F. Revealing the Short-Circuiting Mechanism of Garnet-Based Solid-State Electrolyte. *Adv. Energy Mater.* **2019**, *9*, 1900671.
(29) Fei, H.; Liu, Y.; An, Y.; Xu, X.; Zhang, J.; Xi, B.; Xiong, S.; Feng, J. Safe All-Solid-State Potassium Batteries with Three Dimentional, Flexible and Binder-Free Metal Sulfide Array Electrode. *J. Power Sources* **2019**, *433*, 226697.
(30) Ma, Y.; Doyle, M.; Fuller, T. F.; Doeff, M. M.; De Jonghe, L. C.; Newman, J. The Measurement of a Complete Set of Transport Properties for a Concentrated Solid Polymer Electrolyte Solution. *J. Electrochem. Soc.* **1995**, *142*, 1859−1868.
(31) Bard, A. J.; Faulkner, L. R. *Electrochemical Methods—Fundamentals and Applications*, 1st ed.; Wiley: New York, 1980.

https://dx.doi.org/10.1021/acsami.0c15015
ACS Appl. Mater. Interfaces 2020, 12, 48677−48683